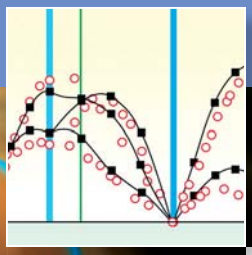

Computational modeling of actinide materials and complexes

Per Söderlind, G. Kotliar, K. Haule, P.M. Oppeneer, and D. Guillaumont

In spite of being rare, actinide elements provide the building blocks for many fascinating condensed-matter systems, both from an experimental and theoretical perspective. Experimental observations of actinide materials are difficult because of rarity, toxicity, radioactivity, and even safety and security. Theory, on the other hand, has its own challenges. Complex crystal and electronic structures are often encountered in actinide materials, as well as pronounced electron correlation effects. Consequently, theoretical modeling of actinide materials and their 5*f* electronic states is very difficult. Here, we review recent theoretical efforts to describe and sometimes predict the behavior of actinide materials and complexes, such as phase stability, including density functional theory (DFT), DFT in conjunction with an additional Coulomb repulsion *U* (DFT+*U*), and DFT in combination with dynamical mean-field theory (DFT+DMFT).

Introduction

The work horse for most condensed-matter calculations is density functional theory (DFT).[1,2] While the theory can be exactly formulated for a homogenous electron gas, it can be applied to any "real-world" material for approximation of the electron exchange and correlation energy (Exc). In view of its humble beginnings, it is remarkably successful in describing the chemical bonding in many elements, compounds, and alloys throughout the periodic table. For example, equilibrium lattice constants are often within 1% of measured values. The local density approximation of the Exc is reasonable for systems with slowly varying electron densities such as *d*-transition metals,[3] while the more recent generalized gradient approximation (GGA) was shown to give a better description[4] of the actinides. Apparently, no GGA can simultaneously be accurate for all atomic properties without sacrificing precision for solids with slowly varying electron densities.[3] This illustrates the difficulty in devising a completely general assumption of the Exc that is applicable for solids with strongly different electron densities.

The atomic volumes of the actinide metals can be used to highlight the difficulties of DFT. In **Figure 1**, the measured atomic volumes for the actinide metals are shown with a black line, the 5*d*-transition metal series with a brown line, and the 4*f* rare-earth series with a green line. We find that the first part of the actinide series shows great similarity to the *d*-transition metal series with a parabolic decrease as a function of atomic number while the second part more resembles that of the rare-earth series. The reason is that the 5*f* electrons are participating in bonding up to Pu, then abruptly withdraw from bonding from Am on, leading to a dramatic volume expansion.

These very distinct trends can roughly be modeled by two extremes, one in which the 5*f* electrons are weakly correlated and forming valence band states and the other with the 5*f* electrons together with the atomic-like core electrons with no inter-atomic bonding. In Figure 1, we show results from calculations that model the band (blue solid circles) and atomic (red squares) limits of the 5*f* electron behavior. The blue solid circles ("5*f* fully bonding") are obtained from electronic-structure calculations with 5*f* electrons treated as weakly correlated and part of the valence band with no other electron interactions than that of the GGA. Notice how well this model reproduces the experimental situation for the early actinides (Th–Np), while for Pu, there is no upturn, as shown experimentally, a fact that is partly due to the lack of spin-orbit coupling in the model.[5]

The red squares are results from calculations identical to the solid blue circles except with the 5*f* electrons confined to core states. This latter extreme in the 5*f* electron behavior gives rise to rather good agreement with the heavier actinides from Am and on while failing for the early actinides. Ideally, of course, one prefers to have an approximation to the Exc, which can handle

Per Söderlind, Condensed Matter and Materials Division, Lawrence Livermore National Laboratory; soderlind@llnl.gov
G. Kotliar, Department of Physics and Astronomy, Rutgers University, Piscataway, NJ 08854, USA; kotliar_AT_physics.rutgers.edu
K. Haule, Department of Physics and Astronomy, Rutgers University, Piscataway, NJ 08854, USA; haule@physics.rutgers.edu
P.M. Oppeneer, Uppsala University, SE-75120 Uppsala, Sweden; peter.oppeneer@fysik.uu.se
D. Guillaumont, French Atomic Energy Commission, Marcoule, France; dominique.guillaumont@cea.fr

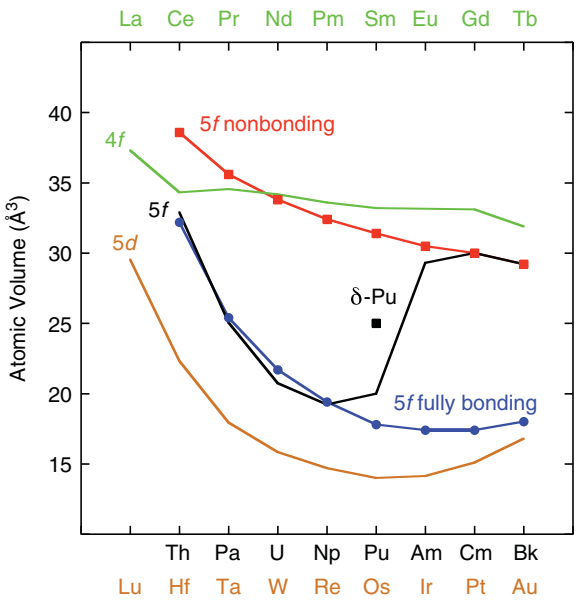

Figure 1. Measured atomic volumes of the actinide metals (5*f*) are shown with a black line, a brown line for the 5*d* transition metals, and a green line for the lanthanides (4*f*). The red "5*f* nonbonding" and blue "5*f* fully bonding" curves show results from model calculations, assuming the face-centered-cubic structure, where the 5*f* electrons are treated as part of the valence band and localized to nonbonding core states, respectively.

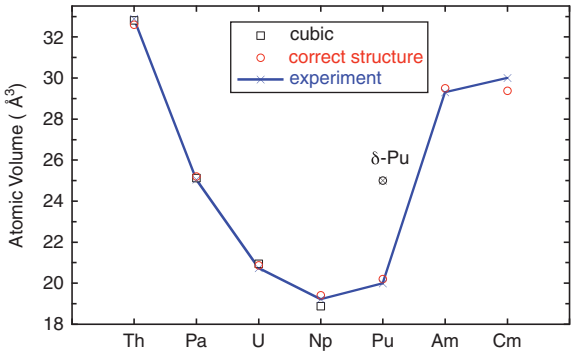

Figure 2. Density functional theory atomic volumes for the actinide metals in the body-centered-cubic and observed crystal structures. The theory is corrected by (experimental) thermal expansion to 300 K except for δ-Pu. Spin-orbit coupling is included for all metals and spin and orbital polarization for δ-Pu, Am, and Cm.[5]

both the band and atomic limits of the 5*f*-electron manner on an equal footing, but current DFT formulations of approximate Exc tend to favor one over the other.[3] In practical DFT calculations for Am, the localized (atomic-like) state of the 5*f* electrons are relatively well modeled by a fully spin-polarized solution, where the spin up (down) manifolds are essentially full (empty) thus removing most of the attractive 5*f* bonding.

Density functional theory results

At one time, the similarity of the light actinides to the *d*-transition series suggested to researchers that the actinides were part of a 6*d* transition series and not a 5*f* transition series.[6] However, our calculations in Figure 1 show clearly that there is an *f* band, with a total of 14 electrons. With this in mind, we display carefully calculated atomic volumes compared with experimental data in **Figure 2**.[5] Notice the rather good agreement between the two sets, suggesting that DFT is a reasonable model for bonding in the actinide metals. The atomic volume reflects an integration of bonding and antibonding states and not necessarily an accurate detailed picture of the electronic structure. For instance, these calculations predict the non-magnetic Am to be magnetic. This is the best DFT solution within the restrictions implied by the GGA for the Exc.

A more sensitive test for the theory is the crystal structure. It depends strongly on details of the electronic structure, particularly close to the Fermi level. Thus, if DFT can reproduce the nontrivial crystal structures in the early actinides (cubic, tetragonal, orthorhombic, and monoclinic), it suggests an accurate DFT electronic structure. About a decade ago, DFT was shown to accomplish this for the early actinides Th–Pu.[7,8] The occurrence of exotic phases, such as monoclinic, is due to narrow 5*f* bands close to the Fermi level that give rise to a Peierls-like distortion that stabilizes low symmetry crystal geometries.[9] The distortion is favorable because degeneracy in electronic states, due to crystal symmetry, can be removed, resulting in a lowering of the energy. During hydrostatic compression, these narrow bands broaden, and the efficiency of the Peierls distortion is diminished while electrostatic interatomic forces of the Madelung-type dictate higher symmetry atomic arrangements. Therefore, one generally observes pressure-induced phase transitions from lower to higher symmetry structures in the actinides. For example, DFT predicted a high-pressure orthorhombic phase of protactinium metal[7] five years before it was confirmed experimentally.[10]

Details of the crystal structures of actinides under compression can be measured using diamond anvil cell techniques. Such findings provide great opportunities to compare models with real data, and in **Figure 3**, we show the *c/a* axial ratio for Ce-Th alloys,[11] with data for uranium[12] in the inset. DFT (open symbols) compares rather well with measured data (filled symbols), suggesting the relevancy of the DFT approach. Another interesting feature of uranium is the low-temperature charge density waves, and DFT calculations by Fast et al.[13] reproduced these waves and their concomitant distortions.

As a function of temperature, Pu metal transforms through six allotropic phases: α, β, γ, δ, δ′, and ε, as shown in the inset of **Figure 4**. Spin-polarized DFT with spin-orbit coupling and orbital polarization captures well this most complex and nontrivial phase diagram, as shown in Figure 4.[14,15] Even though the energies are consistent with the phase diagram (realistic energies and atomic volumes), questions remain regarding the electron correlations and particularly magnetism.[16]

Beyond Pu, the structural behavior of both Am and Cm has been studied by experimental methods[17–20] and DFT calculations,[19–21] and both agree well, implying a robustness of the DFT approach for the heavier actinides. The applicability of DFT for some actinide metals has also been verified by

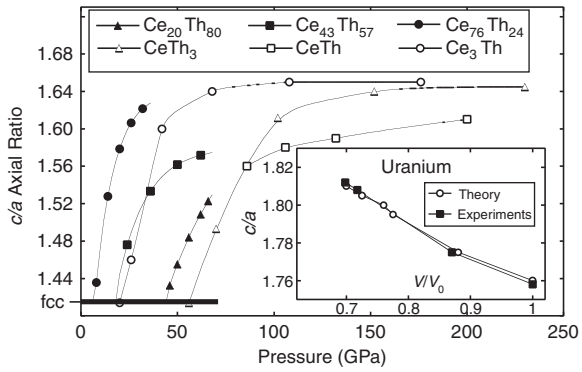

Figure 3. Axial *c/a* ratio as a function of pressure for tetragonal Ce-Th alloys (redrawn from Reference 11). In the inset, we show the *c/a* axial ratio as a function of compression for α-U.[12] Open symbols are density functional theory results, and filled symbols show measured data. *V* is the atomic volume, and V_0 is the atomic volume at equilibrium, or zero pressure.

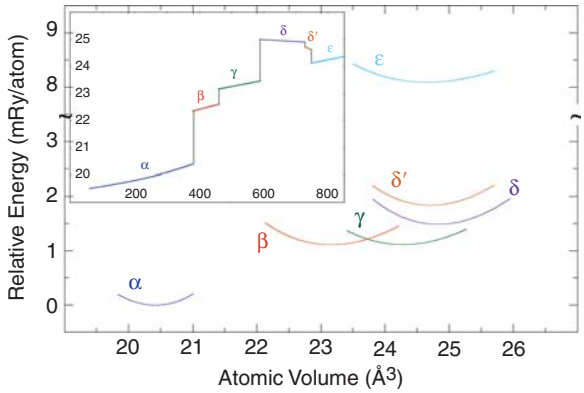

Figure 4. Total energies for Pu.[14,15] The inset shows the experimental volume (Å^3)-temperature (K) phase diagram of Pu metal.

comparisons with experimental data for elastic properties. This has been done for Th,[22,23] U,[24–26] and Pu.[27,28]

Although DFT correctly reproduces many properties of the actinides, the magnetic properties of Pu may be questionable. Clearly, for americium, the magnetic prediction is incorrect and due to the failure of DFT to accurately represent the atomic non-magnetic 5*f*-electron states. Dynamical mean-field theory (DMFT) and DFT in conjunction with Coulomb corrections (DFT+*U*) are suitable to deal with the complete 5*f*-electron localization that occurs for Am in its non-magnetic ground state. An important failure of DFT is the lack of a proper description of the high-temperature body-centered-cubic (bcc) phase that all actinides adopt prior to melting. Standard DFT treatments rely on the Born-Oppenheimer approximation (i.e., frozen atoms corresponding to zero temperature) (and no zero-point motion). For the high-temperature bcc phase, the zero temperature DFT approach predicts mechanical instabilities, rendering DFT problematic for these phases.

For actinide molecular compounds, DFT has become the method of choice in the recent years to compute molecular properties, especially when the systems are too large to be handled by other more computationally demanding *ab initio* approaches. To expand the molecular electron density, basis sets of local functions can be employed. Relativistic effects can be incorporated in effective core potentials that replace core electrons,[29] or they can be included through approximations to the Dirac equation such as the zeroth-order regular approximation.[30] A good test for the theoretical approaches is the correct reproduction of bond distances obtained from crystal structures. Recent work has shown that DFT can provide very good agreement between optimized DFT and crystal structures.[31,32]

The involvement of 5*f* orbitals in bonding has been the subject of much debate and has been largely investigated through DFT calculations. Most of the recent investigations indicate that 5*f* and 6*d* orbitals are both involved in the chemistry of the actinide elements. However, while the 5*f* involvement in the bonding is especially important for uranium, the 5*f* participation in the bonding decreases when moving across the series. Thus, for plutonium, americium, or curium in their trivalent oxidation states, DFT calculations give mostly electronic donation into vacant 6*d* orbitals from atoms present in the actinide environment.[33,34] For actinide molecular compounds, the main limitations of DFT are to properly describe excited properties and energy changes when open-shell actinide systems are involved.

DFT+*U* results

Photoemission spectroscopy experiments are sensitive to the *f* states through the energy-dependent cross-section and reveal that in most light-actinide materials, the 5*f* states are a few eV wide and located near or just below the Fermi level (E_F). Energy positions of 5*f* electrons near or a few eV below E_F imply that the DFT+*U* approach may be used to describe the material's electronic structure. In this approach, an additional on-site Coulomb interaction, expressed by the Coulomb parameter *U* and exchange parameter *J*, is added for the *f* electrons; a subtraction of a so-called double counting term avoids double counting of the mean-field Coulomb interaction already contained in the standard DFT. The Coulomb parameter *U* may vary from 0 eV for delocalized *f*-systems to about 5 eV for rather localized materials such as actinide oxides and the late actinides. Calculations of the *U* parameter have provided values of 2–10 eV for actinide atoms;[35] fits of the Coulomb *U* (e.g., for UO_2) to available experimental data gave $U = 4.5$ eV.[36] The exchange *J* parameter is less well established for actinides; it may vary from $J = 0$ eV to 0.7 eV (see Reference 37). Both the *U* and *J* are related to the Slater integrals $F_{2\kappa}$ ($\kappa = 0, 1, 2, 3$) that describe the full two-electron Coulomb interaction, with $U = F_0$ but $J = J(F_2, F_4, F_6)$. The DFT+*U* approach has been successfully applied to a large number of actinide compounds (e.g., References 38–46).

In some cases, simplified implementations either of the DFT+*U* functional (e.g., Reference 40) or by neglecting simply the spin-orbit (SO) interaction (e.g., References 47 and 48) have been used. Other implementations treat the added +*U* part and SO on an equal footing.[41] Obviously, the neglect of the SO is

rarely justified for actinides, as it is responsible for a splitting of about 1 eV of the $5f_{5/2}$ and $5f_{7/2}$ states.

DFT+U calculations capture the correlated nature of the open 5f shell and produce a different magnetic solution than conventional DFT. For example, for light actinide systems, the +U approach tends to enhance the orbital moment, which is often too small in DFT calculations employing the GGA or local density approximation (LDA). This occurs because the +U scheme has an orbital dependent potential. The improvement is large for insulating actinide oxides, as, for example, UO_2, where the removal of 5f weight from the Fermi level provides correctly an insulating state.[44]

DFT+U calculations, treating the SO interaction and +U part on an equal footing, have predicted a behavior distinct from the DFT. Specifically, LDA+U calculations (using a certain form of the double counting correction) predict a completely non-magnetic state for δ-Pu as well as for Pu-Am alloys.[49,50] **Figure 5a** shows the calculated spin (M_S), orbital (M_L), and total ($M_{tot.}$) moments as a function of the Coulomb U parameter. For reasonable values U = 3–4 eV, LDA+U calculations[49] self-consistently converge to a non-magnetic ground state for δ-Pu. Relativistic LDA+U calculations for other Pu-compounds have also given non-magnetic ground states. One example is the heavy-fermion superconductor $PuCoGa_5$.[51] Figure 5b shows the LDA+U computed energy dispersions of $PuCoGa_5$.[52] The separation of the 5f manifold is clearly seen. In spite of using U = 3 eV, the bands near the Fermi energy E_F are still hybridized, dispersive 5f bands. Hence, the Fermi surface of $PuCoGa_5$ has an appreciable amount of 5f character, and, in addition, it is rather two-dimensional on account of the $HoCoGa_5$ tetragonal structure (see References 46 and 52). Such features are favorable for bringing about the superconductivity observed in $PuCoGa_5$ at a high critical temperature T_c. The most-recent neutron measurements reveal $PuCoGa_5$ to be non-magnetic.[53] This is in agreement with LDA+U calculations, but it is a surprising result from the viewpoint that spin-fluctuations were believed to be responsible for the unusually high T_c in $PuCoGa_5$.[54,55] The reason that the LDA+U scheme tends to predict non-magnetic ground states for Pu and Am compounds has been analyzed.[46,49] The DFT+U method favors a magnetic coupling between the f-electrons that is closer to the atomic limit, whereas plain DFT calculations are normally closer to the Russell-Saunders weak coupling limit. This difference becomes important particularly for Pu and Am (i.e., close to a filled j = 5/2 subshell).

DMFT results

Dynamical mean-field theory (DMFT) has had numerous successes in the field of actinides.[56–70] For example, theoretical prediction of the phonon spectra of δ-Pu[57] were shown to be surprisingly accurate by later inelastic x-ray scattering measurements,[71] both reproduced in **Figure 6**. Considering the approximations involved in the calculations and the fact that δ-Pu is stabilized by small amounts of Ga impurities, the

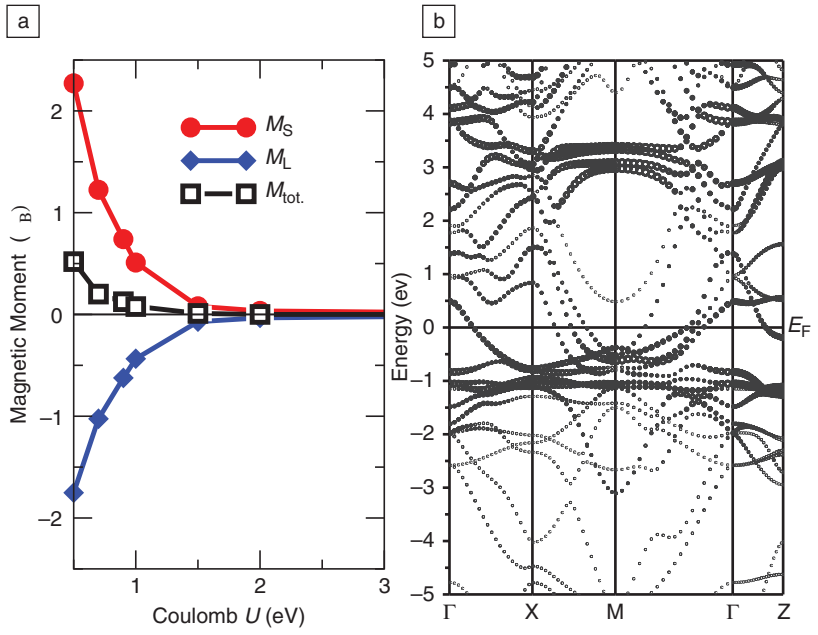

Figure 5. Density functional theory with additional Coulomb repulsion (DFT+U) calculations. (a) Computed spin moment (M_S), orbital moment (M_L), and total moment ($M_{tot.}$) of δ-Pu as a function of the Coulomb U parameter in local density approximation (LDA)+U calculations.[49] (b) Computed energy band dispersions of $PuCoGa_5$ using the LDA+U approach (with Coulomb parameter U = 3 eV and exchange parameter J = 0.6 eV).[52] The size of the circles denotes the amount of 5f character in a band. The high-symmetry points are Γ = (0,0,0), X = (0,1/2,0), M = (1/2,1/2,0), and Z = (0,0,1/2) in reciprocal space units.

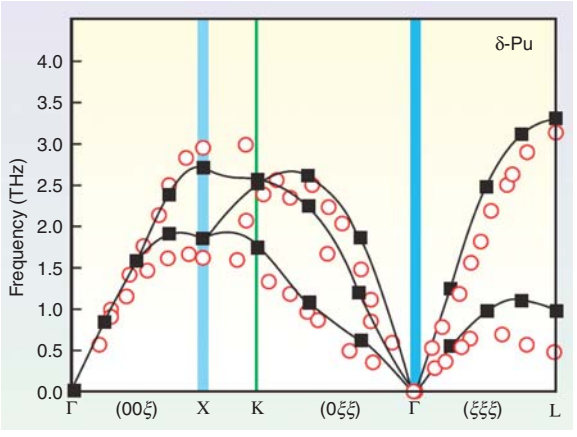

Figure 6. Predicted zero temperature theoretical phonon spectrum of δ-Pu (red) calculated using dynamical mean-field theory compared with experimental values (solid squares) measured at room temperature. The dispersion curves plotted here map the vibrational frequencies of the atoms in momentum space. The frequencies vary with the wave vectors and are evident in the branches as one moves in a particular Brillouin zone direction.[74] Γ, K, X, L, and ξ are high symmetry points in the first Brillouin zone.

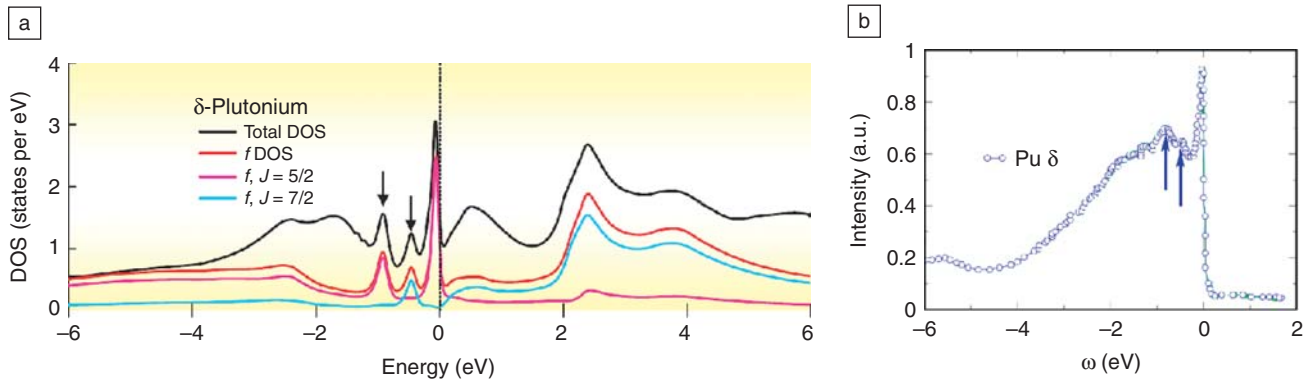

Figure 7. Photoemission spectra of δ-Pu (a) local density approximation (LDA)+ dynamical mean-field theory (DMFT) theory and (b) experiment.[76] Notice the presence of the hubbard bands (atomic-like excitations that have a short lifetime in solids and therefore appear as broad peaks in photoemission spectra) at high energies and the coherent quasiparticle multiplets at low energy, indicated by arrows.[58,63] DOS, density of states; *f*, the orbital angular momentum of an electron; *J*, the total angular momentum, which is the sum of the orbital and spin angular momenta; ω, the energy.

agreement between theory and experiment is good. The photoemission spectra of δ-Pu is also in good agreement with the experimental results, as shown in **Figure 7**.[58,63] Notice the presence of coherent and incoherent spectral weight present in both theory and experiment. Plutonium and its compounds display the phenomena of quasiparticle multiplets (additional structure in the low energy quasiparticle peaks), which are a fingerprint of Pu's mixed-valence character. The quasiparticle multiplets are labeled by arrows in Figure 7. The physical origin of these quasiparticle multiplets and their relation to mixed valence of Pu compounds have been elucidated in Reference 60.

At ambient pressure, DMFT accounts for the non-magnetic state of Am and δ-Pu and the magnetic state of Cm.[58] The boundary of the localization-delocalization transition in elemental Pu was recently explored in Reference 63. The results reveal that a 25 percent volume expansion frees the *f* moment of δ-Pu, in agreement with experimental studies of plutonium hydrides. Alloying Pu with Am does not free the plutonium moment, because the volume expansion is compensated by charge transfer effects (hybridization and level shifts).[64] Further advances in computational facilities and algorithms would allow the extension of these calculations to map the electronic phase diagrams of actinides, their alloys, and oxides that are involved in advanced nuclear fuel cycles.

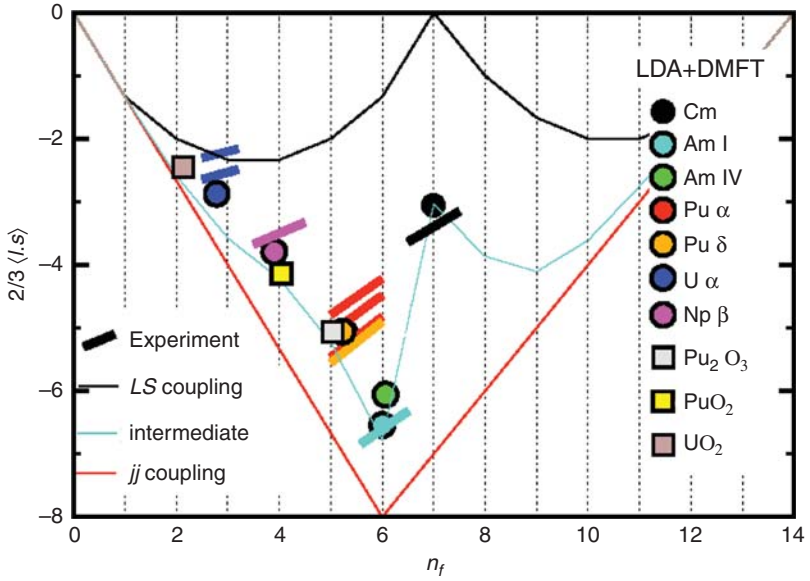

Figure 8. The local density approximation (LDA)+ dynamical mean-field theory (DMFT) expectation value of the angular part of the spin-orbit interaction. The LDA+DMFT results are denoted by circles and rectangles for actinide elements and oxides, respectively.[62] Note: ⟨*l*.*s*⟩ is the average value of the scalar product of two operators, namely *l* and *s*, where *l* is the orbital angular momentum and *s* is the spin angular momentum of an electron; n_f, number of *f* electrons; *L*, total orbital angular momentum; *S*, total spin angular momentum; and *j*, quantum number.

DMFT forms a basis for theoretical spectroscopy, supplementing advanced experimental techniques, to yield new insights in the field of actinides. For example, a recent study addressed the ratio of the two electronic core-valence transitions (between the 4*d* to 5*f* states), which are measured in electron energy-loss and x-ray absorption spectroscopy, across the actinide series.[62] The results are reproduced in **Figure 8**, which are in agreement with experimental results.[72,73] Experimentally, only one quantity is measured, the branching ratio. This quantity is determined by two parameters, the *f*-occupancy and the strength of the spin-orbit coupling. These two parameters are separately accessible in local density approximation (LDA) +DMFT and can be used to determine the value of the branching ratio. These studies were crucial in elucidating the Pu valence, which is mixed valent, hence non-integer, but close to $5f^5$. The DMFT technique is currently applied to actinide materials by many groups around the world. These works are too numerous

to cite, and we can only provide a partial list of references[56–70] and recent reviews.[74,75]

Conclusions

Recent theoretical and computational advances have resulted in more accurate and realistic calculations of the complex electronic structure of actinide materials. We have surveyed a series of methods, which describe actinides effects with increasing level of complexity (LDA, LDA+*U*, LDA+DMFT) at increasing computational cost. These developments are already giving new exciting insights into the fundamental physics of these materials. Further developments are under way to improve the accuracy of the exchange correlation potentials in DFT to obtain higher accuracy in the total energies, while new algorithms are under development to accelerate the computational speed and accuracy of LDA+DMFT total energy and spectra. Predictive theories of complex actinide materials are well within reach.

Acknowledgments

This work performed under the auspices of the U.S. DOE by LLNL under Contract DE-AC52-07NA27344. G.K. was supported by DOE-BES DE-FGO2-99ER45761.

References

1. P. Hohenberg, W. Kohn, *Phys. Rev.* **136**, B864 (1964).
2. W. Kohn, L. Sham, *Phys. Rev.* **140**, A1133 (1965).
3. J.P. Perdew, A. Ruzsinsky, G.I. Csonka, O.A. Vydorv, G.E. Scuseria, L.A. Constantin, X. Zhou, K. Burke, *Phys. Rev. Lett.* **100**, 136406 (2008).
4. P. Söderlind, O. Eriksson, B. Johansson, J.M. Wills, *Phys. Rev. B* **50**, 7291 (1994).
5. P. Söderlind, C.S. Nash, in Advances in Plutonium Chemistry *1967–2000,* D. Hoffman, Ed. (American Nuclear Society, La Grange Park, 2002), p. 14.
6. W.H. Zachariasen, *J. Inorg. Nucl. Chem.* **35**, 3487 (1973).
7. P. Söderlind, *Adv. Phys.* **47**, 959 (1998).
8. M. Penicaud, J. *Phys. Condens. Matter* **12**, 5819 (2000).
9. P. Söderlind, O. Eriksson, B. Johnasson, J.M. Wills, B. Johansson, *Nature* **374**, 524 (1995).
10. R.G. Haire, S. Heathman, M. Iridi, T. Le Bihan, A. Lindbaum, J. Rebizant, *Phys. Rev. B* **67**, 134101 (2003).
11. P. Söderlind, O. Eriksson, *Phys. Rev. B* **60**, 9372 (1999).
12. J. Akella, S. Weir, J.M. Wills, P. Söderlind, *J. Phys. Condens. Matter* **9**, L549 (1997).
13. L. Fast, O. Eriksson, B. Johansson, J.M. Wills, G. Straub, H. Roeder, L. Nordström, *Phys. Rev. Lett.* **81**, 2978 (1998).
14. P. Söderlind, *Europhys. Lett.* **55**, 525 (2001).
15. P. Söderlind, B. Sadigh, *Phys. Rev. Lett.* **92**, 185702 (2004).
16. J.C. Lashley, A. Lawson, R.J. McQueeney, G.H. Lander, *Phys. Rev. B* **72**, 054416 (2005).
17. S. Heathman, R.G. Haire, T. Le Bihan, A. Lindbaum, K. Litfin, Y. Meresse, H. Libotte, *Phys. Rev. Lett.* **85**, 2961 (2000).
18. A. Lindbaum, S. Heathman, K. Litfin, Y. Meresse, R.G. Haire, T. Le Bihan, H. Libotte, *Phys. Rev. B* **63**, 214101 (2001).
19. S. Heathman, R.G. Haire, T. Le Bihan, A. Lindbaum, M. Iridi, P. Normile, S. Li, R. Ahuja, B. Johansson, G.H. Lander, *Science* **309**, 110 (2005).
20. K.T. Moore, G. van der Laan, R.G. Haire, M.A. Wall, A.J. Schwartz, P. Söderlind, *Phys. Rev. Lett.* **98**, 236402 (2007).
21. P. Söderlind, A. Landa, *Phys. Rev. B* **72**, 024109 (2005).
22. P. Söderlind, O. Eriksson, J.M. Wills, A.M. Boring, *Phys. Rev. B* **48**, 9306 (1993).
23. J. Bouchet, F. Jollet, G. Zerah, *Phys. Rev. B* **74**, 134304 (2006).
24. P. Söderlind, *Phys. Rev. B* **66**, 085113 (2002).
25. J. Bouchet, *Phys. Rev. B* **77**, 024113 (2008).
26. C.D. Taylor, *Phys. Rev. B* **77**, 094119 (2008).
27. P. Söderlind, J.E. Klepeis, *Phys. Rev. B* **79**, 104110 (2009).
28. P. Söderlind, A. Landa, J.E. Klepeis, Y. Suzuki, A. Migliori, *Phys. Rev. B* **81**, 224110 (2010).
29. P.J. Hay, R.L. Martin, *J. Chem. Phys.* **109**, 3875 (1998).
30. E. van Lenthe, E.J. Baerends, J.G. Snijders, *J. Chem. Phys.* **99**, 4597 (1993).
31. E.J. Schelter, P. Yang, B.L. Scott, R.E. Da Re, K.C. Jantunen, R.L. Martin, P.J. Hay, D.E. Morris, J.L. Kiplinger, *J. Am. Chem. Soc.* **129**, 5139 (2007).
32. I. Charushnikova, E. Bosse, D. Guillaumont, P. Moisy, *Inorg. Chem.* **49**, 2077 (2010).
33. K.I.M. Ingram, M.J. Tassell, A.J. Gaunt, N. Kaltsoyannis, *Inorg. Chem.* **47**, 7824 (2008).
34. D. Guillaumont, *J. Phys. Chem. A* **108**, 6893 (2004).
35. J.F. Herbst, R.E. Watson, I. Lindgren, *Phys. Rev. B* **14**, 3265 (1976).
36. S.L. Dudarev, D. Nguyen Manh, A.P. Sutton, *Philos. Mag. B* **75**, 613 (1997).
37. D. van der Marel, J. Sawazky, *Phys. Rev. B* **37**, 10674 (1988).
38. P.M. Oppeneer, A.N. Yaresko, A.Y. Perlov, V.N. Antonov, H. Eschrig, *Phys. Rev. B* **54**, R3706 (1996).
39. P.M. Oppeneer, V.N. Antonov, A.Y. Perlov, A.N. Yaresko, T. Kraft, H. Eschrig, *Physica B* **230** (232), 544 (1997).
40. S.L. Dudarev, G.A. Botton, S.Y. Savrasov, C.J. Humphreys, A.P. Sutton, *Phys. Rev. B* **57**, 1505 (1998).
41. A.B. Shick, A.I. Liechtenstein, W.E. Pickett, *Phys. Rev. B* **60**, 10763 (1999).
42. S.Y. Savrasov, G. Kotliar, *Phys. Rev. Lett.* **84**, 3670 (2000).
43. A.B. Shick, W.E. Pickett, *Phys. Rev. Lett.* **86**, 300 (2001).
44. R. Laskowski, G.K.H. Madsen, P. Blaha, K. Schwarz, *Phys. Rev. B* **69**, 140408(R) (2004).
45. D.B. Ghosh, S.K. De, P.M. Oppeneer, M.S.S. Brooks, *Phys. Rev. B* **72**, 115123 (2005).
46. A.B. Shick, V. Janis, P.M. Oppeneer, *Phys. Rev. Lett.* **94**, 016401 (2005).
47. I.D. Prodan, G.E. Scuseria, R.L. Martin, *Phys. Rev. B* **76**, 033101 (2007).
48. B.-T. Wang, H. Shi, W. Li, P. Zhang, *Phys. Rev. B* **81**, 045119 (2010).
49. A.B. Shick, V. Drchal, L. Havela, *Europhys. Lett.* **69**, 588 (2005).
50. A.B. Shick, L. Havela, J. Kolorenc, V. Drchal, T. Gouder, P.M. Oppeneer, *Phys. Rev. B* **73**, 104415 (2006).
51. J.L. Sarrao, L.A. Morales, J.D. Thompson, B.L. Scott, G.R. Stewart, F. Wastin, J. Rebizant, P. Boulet, E. Colineau, G.H. Lander, *Nature* **420**, 297 (2002).
52. P.M. Oppeneer, A.B. Shick, J. Rusz, S. Lebegue, O. Eriksson, *J. Alloys Compd.* **444–445**, 109 (2007).
53. A. Hiess, A. Stunault, E. Colineau, J. Rebizant, F. Wastin, R. Caciuffo, G.H. Lander, *Phys. Rev. Lett.* **100**, 076403 (2008).
54. I. Opahle, P.M. Oppeneer, *Phys. Rev. Lett.* **90**, 157001 (2003).
55. E.D. Bauer, J.D. Thompson, J.L. Sarrao, L.A. Morales. F. Wastin, J. Rebizant, J.C. Griveau, P. Javorsky, P. Boulet, E. Colineau, G.H. Lander, G.R. Stewart, *Phys. Rev. Lett.* **93**, 147005 (2004).
56. S. Savrasov, G. Kotliar, E. Abrahams, *Nature* **410**, 793 (2001).
57. X. Dai, S.Y. Savrasov, G. Kotliar, A. Migliori, H. Ledbetter, E. Abrahams, *Science* **300**, 953 (2003).
58. J.H. Shim, K. Haule, G. Kotliar, *Nature* **446**, 513 (2007).
59. J.H. Shim, K. Haule, S. Savrasov, G. Kotliar, *Phys. Rev. Lett.* **101**, 126403 (2008).
60. C.-H. Yee, G. Kotliar, K. Haule, *Phys. Rev. B* **81**, 035105 (2010).
61. K. Haule, G. Kotliar, *Nat. Phys.* **5**, 796 (2009).
62. J.H. Shim, K. Haule, G. Kotliar, *Europhys. Lett.* **85**, 17007 (2009).
63. C.A. Marianetti, K. Haule, G. Kotliar, M.J. Fluss, *Phys. Rev. Lett.* **101**, 056403 (2008).
64. S.Y. Savrasov, K. Haule, G. Kotliar, *Phys. Rev. Lett.* **96**, 036404 (2006).
65. M.J. Han, X. Wan, S.Y. Savrasov, *Phys. Rev. B* **78**, 060401 (2008).
66. L.V. Pourovskii, M.I. Katsnelson, A.I. Lichtenstein, L. Havela, T. Gouder, F. Wastin, A.B. Shick, V. Drchal, G.H. Lander, *Europhys. Lett.* **74**, 479 (2006).
67. L.V. Pourovskii, M.I. Katsnelson, A.I. Lichtenstein, *Phys. Rev. B* **72**, 115106 (2005).
68. M.-T. Suzuki, P.M. Oppeneer, *Phys. Rev. B* **80**, 161103 (2009).
69. L.V. Pourovskii, M.I. Katsnelson, A.I. Lichtenstein, *Phys. Rev. B* **73**, 060506 (2006).
70. J.-X. Zhu, A.K. McMahan, M.D. Jones, T. Durakiewicz, J.J. Joyce, J.M. Wills, *Phys. Rev. B* **76**, 245118 (2007).
71. J. Wong, M. Krisch, D.L. Farber, F. Occelli, A.J. Schwartz, T.-C. Chiang, M. Wall, C. Boro, R.Q. Xu, *Science* **301**, 1078 (2003).
72. K.T. Moore, G. van der Laan, M.A. Wall, A.J. Schwartz, R.G. Haire, *Phys. Rev. B* **76**, 073105 (2007).
73. K.T. Moore, G. van der Laan, Rev. Mod. Phys. 81, 235 (2009).
74. G. Kotliar, D. Vollhardt, *Phys. Today* **57**, 53 (2004).
75. G. Kotliar, S.Y. Savrasov, K. Haule, V.S. Oudovenko, O. Parcollet, C.A. Marianetti, *Rev. Mod. Phys.* **78**, 865 (2006).
76. A.J. Arko, J.J. Joyce, L. Morales, J. Wills, J. Lashley, F. Wastin, J. Rebizant, *Phys. Rev. B* **62**, 1773–1779 (2000). □

"Want Your Research Published Faster?"

THE JOURNAL OF PHYSICAL CHEMISTRY Letters

Editor-In-Chief:
George C. Schatz
Northwestern University

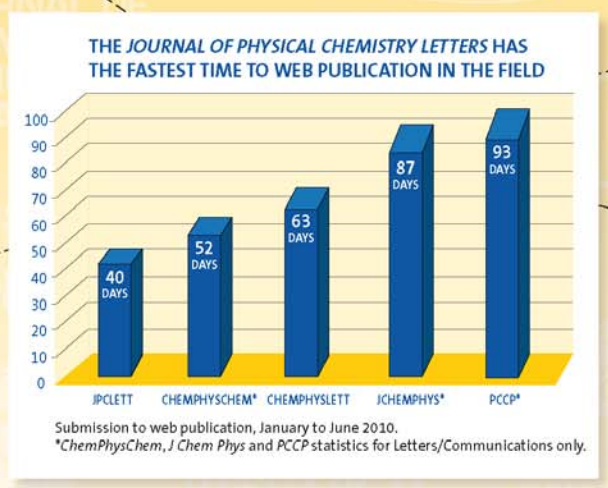

4-6 WEEKS SUBMISSION TO WEB PUBLICATION

Deputy Editor:
Prashant V. Kamat
University of Notre Dame

Don't Get Scooped!

When you've produced cutting-edge results in physical chemistry, you want your research published in record time. With the *Journal of Physical Chemistry Letters*, authors gain the benefits of:

- Rapid publication, with submission to web publication in just 4 to 6 weeks
- Cite at first sight – full citation, with page numbers, when articles first appear on the web
- High visibility and broad worldwide distribution

Go to pubs.acs.org/JPCL

See why the *Journal of Physical Chemistry Letters* has quickly become the go-to journal to publish and discover urgent results in physical chemistry — with Letter submissions to *JPC* doubling since the launch of the new journal. And check out the library of videos created by Perspective authors, giving viewers new insights on their research.

ACS Publications
MOST TRUSTED. MOST CITED. MOST READ.

pubs.acs.org